Surface & Coatings Technology 397 (2020) 126048

Contents lists available at ScienceDirect

Surface & Coatings Technology

journal homepage: www.elsevier.com/locate/surfcoat

Anti-wear Cr-V-N coating via V solid solution: Microstructure, mechanical and tribological properties

Beibei Xu[a,b], Peng Guo[a], Zhenyu Wang[a], Rende Chen[a], Yumin Ye[b], Jintao Shuai[a], Aiying Wang[a,c,*], Peiling Ke[a,c,*]

[a] Key Laboratory of Marine Materials and Related Technologies, Zhejiang Key Laboratory of Marine Materials and Protective Technologies, Ningbo Institute of Materials Technology and Engineering, Chinese Academy of Sciences, Ningbo 315201, China
[b] Faculty of Materials Science and Chemical Engineering, Ningbo University, Ningbo 315211, China
[c] Center of Materials Science and Optoelectronics Engineering, University of Chinese Academy of Sciences, Beijing 10049, China

ARTICLE INFO

Keywords:
Cr-V-N
Solid solution
Microstructure
Mechanical property
Anti-wear

ABSTRACT

V-containing solid solution was considered as a promising way to improve the mechanical and tribological properties of hard coatings due to the mechanism of solid solution as well as the induced V-based Magnéli lubricant during friction process. In this work, Cr-V-N coatings with different V contents were prepared on polished cemented carbide and P-type Si (100) wafers by cathodic arc evaporation. The microstructure, mechanical and tribological properties of the coatings with varied V content were discussed. When the content ranged from 0.32 to 31.14 at.%, V entered into the lattice of CrN crystal in the form of solid solution without affecting the coating's phase composition. CrN phase with (111) orientation was formed for all Cr-V-N coatings, and the coating with 31.14 at.% V content showed the weakest crystallinity. The introduction of V still retained the composited coatings with high toughness and excellent adhesion strength of around 100 N on cemented carbide substrates. The maximum elastic modulus and hardness reached up to 438.5 ± 5.3 GPa and 20.0 ± 1.0 GPa, respectively, with V content at 16.55 at.%. Tribological tests at room temperature demonstrated that the friction coefficient of Cr-V-N coatings was relatively low, which was between 0.26 and 0.36. The wear rate was in the order of magnitude of 10^{-7} mm^{3}N^{-1} m^{-1}, and the lowest wear rate was 2.5×10^{-7} mm^{3}N^{-1} m^{-1} with V content at 0.32 at.%. The friction coefficient and wear rate both increased with the increase of V content. The wear rate of the coatings with high V content (31.14 at.%) was almost four times higher than that of low V content (0.32 at.%) coatings.

1. Introduction

Lubricating coatings with good tribological properties are of great need for cutting tools, machinery components and transportation fields in modern industry. Recent attention to pollution prevention and cost saving has accelerated incentives for the application of solid lubricating coatings, especially transition metal nitride (TMN) hard coatings, to replace the oil and grease lubrication. Among these coatings, CrN has been attracting intensive attention due to its superior performance under harsh environmental exposure, such as high hardness, low internal stress, anti-corrosion, good environmental adaptation and chemical inertness [1–3]. Nevertheless, its high friction coefficient (COF) of 0.5–0.7 under dry conditions [4] limits its applications.

Xu et al. [5] suggested that Cr and V elements have similarities in the profiles of the density of states (DOS), and the crystal structure of CrN is akin to that of VN. So, these two elements show a complete series of solid solution rather than any compound [6], which will contribute to the improvement of the strength of the materials. Moreover, V_2O_5, a typical oxide of V, is easy to form during the friction process. It belongs to a kind of Magnéli oxide phase and is normally considered as the lubricating phase due to its easy crystallographic shear feature. Wang et al. [7] reported that the V_2O_5 formed during the friction process of VAlCN coating at room temperature, and the high hardness as well as the improved toughness of the coating jointly resulted in low friction coefficient and good wear resistance. Therefore, to obtain the combined self-lubricating and anti-wear effects at room temperature, adding V element into CrN coatings to form ternary Cr-V-N solid solution coating becomes an attracting choose. As discussed above, CrN is selected as the

---

[*] Corresponding authors at: Key Laboratory of Marine Materials and Related Technologies, Zhejiang Key Laboratory of Marine Materials and Protective Technologies, Ningbo Institute of Materials Technology and Engineering, Chinese Academy of Sciences, Ningbo 315201, China.
E-mail addresses: aywang@nimte.ac.cn (A. Wang), kepl@nimte.ac.cn (P. Ke).

https://doi.org/10.1016/j.surfcoat.2020.126048
Received 7 March 2020; Received in revised form 29 May 2020; Accepted 7 June 2020

base material in this study, V element is added as the lubricious material, and the formation of solid solution phase is expected to strengthen the mechanical property. A combination of the basic phase, the reinforced phase and the lubricating phase is expected to have a synergetic effect to endow the coating with superior mechanical and tribological properties.

It is generally recognized that the addition of heterogeneous atoms to a solid solution will cause the distortion of the crystal lattice, thereby improving the strength of the materials. Tian et al. [8] prepared the nearly dense $(Cr_{1-x}V_x)_2AlC$ (x = 0, 0.1, 0.25 and 0.5) solid solutions and found that the addition of V caused linear increase of Vickers hardness benefiting from the solid-solution strengthening effect. Similar results were also observed for $(Ti, V)_2AlC$ [9], $(Ti, Nb)_2AlC$ [10], $CoCrFeNiVAl_x$ [11]. However, the effects of heterogeneous solid solution atoms on mechanical and tribological properties have been in the contradictory statement. Wo et al. [12] constructed the $Ti_3Al_{1.2-x}Si_xC_2$ solid solution and the enhanced Si doping led to an increased hardness, but slightly decreased fracture toughness and increased friction coefficient. Therefore, V content is an indispensable factor to investigate the tribological properties of Cr-V-N coatings.

Although some studies have focused on the tribological properties of CrVN system, the influence of the V content on mechanical and tribological properties of the Cr-V-N coating remains controversial. Aissani et al. [13] reported an obvious decrease in friction from 0.52 to 0.39, and simultaneously a reduction in hardness from 11.0 GPa to 6.2 GPa when the V content was improved from 10 at.% to 38 at.%. Whereas, due to the extremely low hardness, the coating quickly worn out with the V content at 38 at.%. Conversely, by using the same deposition technique, the tribological properties of the CrV(35)N coating at room temperature were reported to have been improved due to its smooth virgin surface, high hardness and toughness as well as a small grain size in comparison with the CrV(0)N coating [14,15]. In addition, Uchida et al. [16] found that the hardness of $Cr_{50}V_{50}N$ coatings deposited by cathodic arc ion plating was 15 GPa, equal to that of the CrN coating. In terms of the CrN/VN coating with 11.5 at.% V content and CrN coating, the variations of hardness and friction coefficient were not pronounced, reported by Qiu et al. [17]. Overall, it is necessary to further investigate the influence of the V content on mechanical and tribological properties of the Cr-V-N coating, and clarify the friction mechanism.

In this work, arc-evaporated Cr-V-N coatings with different V contents were prepared, and the microstructure, mechanical and tribological properties at room temperature of them were systematically studied. Additionally, whether the oxide scales formed during friction process at room temperature was also revealed.

2. Experimental details

2.1. Sample preparation

Cr-V-N coatings with different V contents were prepared on polished cemented-carbide (15 mm × 15 mm × 3 mm) and P-type Si (100) wafers by cathodic arc evaporation. The cemented carbide was YG8, and the nominal composition (wt%) was: WC-92, Co-8. Before deposition, the cemented carbide substrate was mirror polished to obtain the surface roughness (Ra) of ~0.006 μm. Cr-V-N coatings were co-deposited at N_2 atmosphere by using the purity of 99.99 wt% Cr (φ128 mm × 15 mm) and V (φ128 mm × 15 mm) targets, which were set vertically in cylindrical vacuum chamber wall. Polished cemented-carbides and Si wafers were mounted on a one-axis rotational fixture facing the two targets, with the rotation speed of 9.5 rpm. The V content of the coating was tuned by varying the substrate position on the one-axis rotational fixture. A schematic diagram of the deposition system is shown in Fig. 1a. The Cr target was fixed above the V target. The vertical distance between the centers of the two cathode targets was 133 cm, and the horizontal distance between targets and the substrates was 15 cm. Fig. 1b presented the distances among the samples. The mean distance between adjacent samples among S1-S3 was 2.5 cm. The evaporation rate of V was higher than that of Cr in this work. In order to avoid the deposition of high V content coatings, the distance between adjacent samples among S3–S6 was evenly set as 1 cm. Prior to deposition, the substrates were ultrasonically cleaned in acetone and ethanol for 10 min, respectively. The deposition temperature of the chamber was maintained at 450 °C and a base pressure of the chamber was pumped down to 3.3×10^{-3} Pa. To improve the adhesion strength between the substrates and coatings, all substrates were firstly etched by Ar^+ bombardments for 60 min to remove oxides and other contaminants on the surface. Then both the thin Cr and CrN interlayer were successively deposited for 8 min in ambient Ar and N_2, respectively. During deposition process, the deposition time was set at 150 min for all Cr-V-N coatings. More detailed deposition parameters are presented in Table 1.

2.2. Characterizations

The surface morphology and cross-sectional microstructure of Cr-V-N coatings were studied by field emission scanning electron microscope (SEM, Quanta FEG 250 and Hitachi S4800). The chemical composition was measured by energy-dispersive X-ray spectroscopy (EDS, OXFORD X-Max). The surface roughness (Ra) of the coatings was measured by laser confocal scanning microscope (Zeiss-material type, Germany) within the fields of 120 × 120 μm². Phase composition of coatings was investigated by X-ray diffraction (XRD, Bruker AXS D8 Advance, Germany) using a Cu Kα radiation with scanning angle ranged from 5 to 90°. The lattice parameter (a) of an identified cubic phase was calculated using the equation $a = d_{hkl}/(h^2 + k^2 + l^2)$, where d was the spacing parameter calculated for (hkl) plane position. The average crystalline size (D) was calculated using the Debye-Scherrer formula [18] as an average of 3 main peaks. The equation was $D = 0.9\lambda_{cu}/(\beta \cos\theta_{hkl})$, where λ_{cu} was 0.514 nm, β was the full width at half maximum (FWHM) of the diffraction lines estimated using Jade software, and θ_{hkl} was the angle of the most intense diffraction line. Chemical bonding state was characterized through X-ray photoelectron spectroscopy (XPS, Axis Ultra DLD, Japan) with Al mono Kα radiation at pass energy of 160 eV. The Cr 2p level at 575.6 eV for CrN was used as reference for energy calibration during data analysis. High-resolution transmission electron microscopy (HRTEM, Talos F200X, USA) was employed for analyzing more detailed microstructure. Before TEM test, the samples were prepared by a focused ion beam system (FIB, Zeiss Auriga, Germany) to obtain the cross-section sample.

The load bearing capacity of coatings and the adhesive strength between coatings and substrates were measured by CSM scratch tester with a tapered diamond tip of 0.2 mm radius and 120° cone angle. The tip moved at a speed of 1.5 mm/min and the scratch length was 3 mm. Simultaneously, the applied load increased linearly from 0 to 180 N at the loading velocity of 90 N/min. The critical load corresponding to the coating started to detach from the substrate (Lc2) was taken as the interfacial adhesive strength. The hardness and elastic modulus of coatings were measured using continuous stiffness mode by MTS Nano Indenter G200 system, equipped with a 20-nm-radius Berkovich diamond tip. The maximum load ranged from 67 to 167 mN and pure aluminum was applied to calibrate the equipment. Before test, the surface roughness of the coatings was polished to < 50 nm, analyzed by scanning white light interference microscope (3D Universal Profilometer, Rtec) within the area of 120 × 120 μm². The maximum depth of penetration was 1000 nm and six repeated indentations in different areas were performed to minimize the measurement error. Loading and unloading were performed for 230 s and 30 s, respectively, with a holding period of 12 s at the maximum load. The value of Young's modulus was determined according to Oliver-Pharr method [19]. The MVS-1000D1 Vickers indenter with the applied load of 5 N was used to identify the toughness of Cr-V-N coatings, and the toughness was evaluated by comparing the micromorphology of indentation.

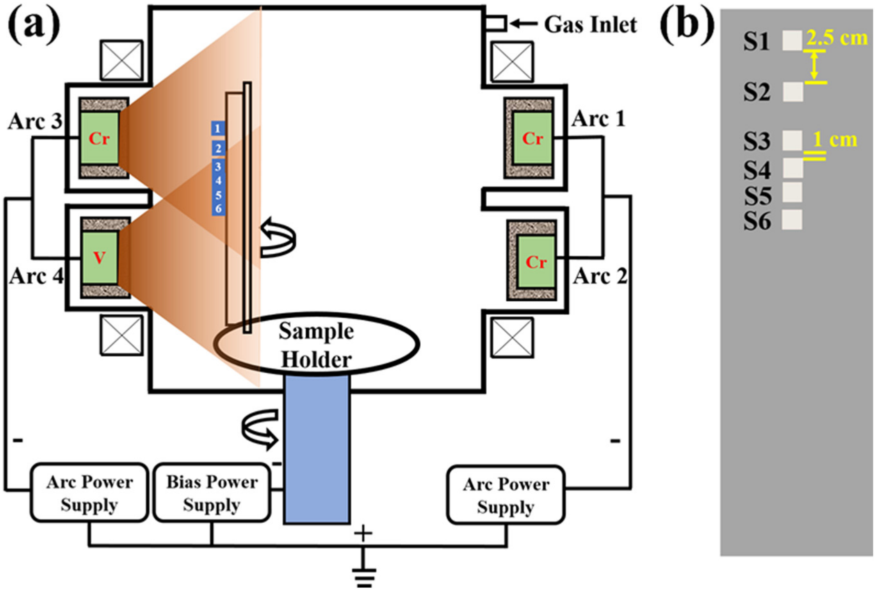

Fig. 1. Schematic diagrams of the arc evaporation system for Cr-V-N coatings (a), and the distances among the samples (b).

Table 1
Detailed deposition parameters.

	Bias voltage (V)	Current (A)			Chamber pressure (Pa)	Ar flow (sccm)	N_2 flow (sccm)	Deposition time (min)
		Ion beam	Cr cathode	V cathode				
Etching	−100	0.2	–	–	–	40	–	60
Cr layer	−200	–	70	–	3	200	–	8
CrN layer	−60	–	70	–	7	–	550	8
CrVN layer	−80	–	70	70	9	–	550	150

Generally, the coating with a small number of circumferential cracks and without radial cracks in the indentation was considered to be with good toughness.

Tribological properties were performed on reciprocating ball-on-disk dry sliding tester (CETR UMT-3MT) under atmospheric environments, and Al_2O_3 balls with a diameter of 6 mm was used as the counter body. A constant load of 5 N with a sliding stroke of 5 mm was applied in the experiment, and the frequency and sliding velocity were set at 5 Hz and 50 mm/s, respectively. After the tribo-test, the wear track profiles were measured by Alpha-Step IQ profile meter. The wear rate (K) was calculated by the formula $K = V/FL$, where V is the wear volume of coatings in mm^3, F is the normal load applied in N, L is the sliding distance in m. Wear debris were analyzed by Raman spectroscopy (In Via-reflex, Renishaw) with 532 nm exciting wavelength laser.

3. Results and discussion

3.1. Chemical composition and microstructure

The chemical composition of the as-deposited Cr-V-N coatings characterized by EDS analysis is summarized in Table 2, where the sample ID is labeled as S1–S6 with increasing V content. The thickness of the coatings ranged from 4.61 to 7.53 μm. Obviously, as the location of samples approached to the V target, the V content of the Cr-V-N coatings gradually increased from nearly 0.32 to 31.14 at.%, accompanied by a decrease in Cr content. In addition, the oxygen impurities were found to be in the range of 0.6–1.4 at.%, which was probably a consequence of the mediocre vacuum degree during deposition process [20].

Fig. 2 presents the surface morphologies of Cr-V-N coatings on cemented carbide. Numerous droplets and micro-pits in different dimension were observed from all coatings, which was a typical feature of the arc-evaporated coating. With the increase of the V content, the number of droplets and micro-pits as well as the particle size increased.

Table 2
The chemical composition, thicknesses and surface roughness of as-deposited Cr-V-N coatings.

Sample ID.	Chemical composition (at.%)				Thickness (μm)	Roughness (μm)
	Cr	V	N	O		
S1	71.40 ± 0.11	0.32 ± 0.03	27.00 ± 0.19	1.27 ± 0.05	7.53	0.172 ± 0.011
S2	71.48 ± 0.45	0.89 ± 0.09	26.65 ± 0.23	0.98 ± 0.13	6.67	0.169 ± 0.010
S3	67.91 ± 0.06	4.46 ± 0.15	27.03 ± 0.12	0.60 ± 0.09	5.14	0.202 ± 0.005
S4	55.23 ± 0.23	11.16 ± 0.37	32.21 ± 0.32	1.40 ± 0.19	4.83	0.213 ± 0.014
S5	54.33 ± 0.04	16.55 ± 0.17	28.10 ± 0.40	1.02 ± 0.61	4.61	0.215 ± 0.019
S6	38.60 ± 2.29	31.14 ± 1.28	29.57 ± 2.39	0.70 ± 0.23	5.48	0.262 ± 0.008

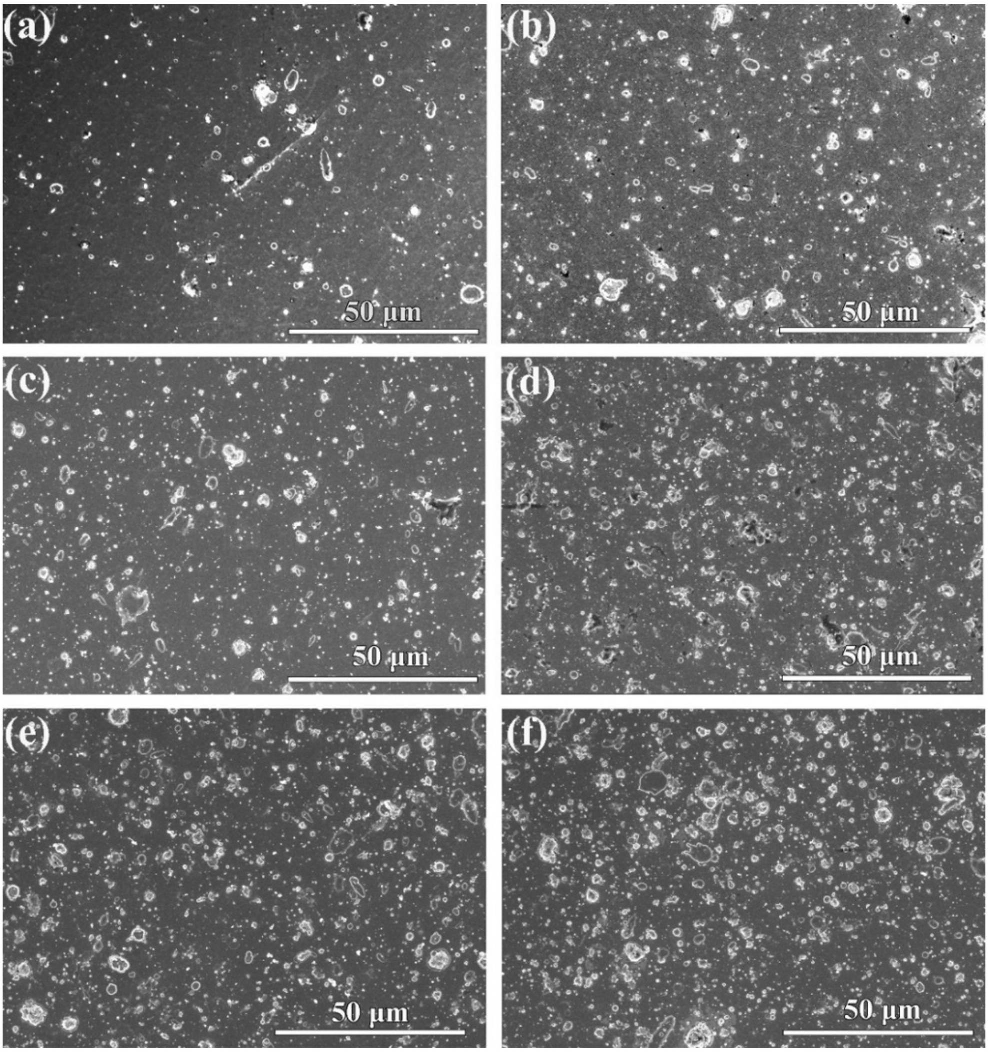

Fig. 2. Surface morphologies of Cr-V-N coatings with different V contents: (a) S1 (0.32 at.%), (b) S2 (0.89 at.%), (c) S3 (4.46 at.%), (d) S4 (11.16 at.%), (e) S5 (16.55 at.%), (f) S6 (31.14 at.%).

Samples with high V content located between the Cr and V targets, where large droplets might overshoot due to the low angle to the target surfaces. The presence of droplets led to considerable surface roughness and the decreased surface finish. The surface roughness (Ra) listed in Table 2 increased from 0.172 μm of S1 to 0.262 μm of S6. This would have adverse effects on mechanical and tribological properties of the coatings.

From cross-sectional SEM micrographs in Fig. 3, the grains with compact columnar structure grew perpendicular to the substrate. Some droplets developed through the coating, leading to the creation of voids labeled in yellow line in Fig. 3e. The columnar structures became coarser along the growth direction and formed V-shaped columns (labeled with yellow arrows in Fig. 3a). This was related to the deposition temperature, the melting point of the material and the effect of additives, as reported by Petrov et al. [21]. The ratio of deposition temperature (Ts = 723 K) to melting point (Tm ≈ 2043 K) was about 0.35. The average kinetic energy of ions (E_i) corresponded approximately to the applied negative substrate bias, that was 80 eV. In this condition, the grain boundaries in the coatings were immobile, and the significantly diffusing of adatoms to the surface gave rise to local epitaxial growth on individual grains. So, the columnar structures developed in the form of elongated grains.

Fig. 4 shows the XRD patterns of the coatings deposited on Si substrates. The Cr metal and CrN phase were detected in the coatings with V content (S1–S6) ranged from 0.32 to 31.14 at.%. CrN exhibited NaCl-type face centered cubic structure with identified diffraction peaks of (111), (200), (220), (311), (222), and (111) preferred orientation growth was recognized. With the increase of V content, the peaks of CrN phase both shifted toward a high angle, whereas, the peak position of Cr metal remained unchanged. The influence of macro residual stress could be ruled out, due to the reason that the peak shift caused by macro residual stress was only for a few or individual high-angle diffraction peaks. The element doping became the leading factor to the right shifting of CrN peaks. Fig. 4b shows the zoomed-in view of (111) peak of CrN. The peak position shifted toward a higher diffraction angle with increasing V content, suggesting both the interplanar spacing and lattice parameters got smaller. The lattice parameter (a) and grain size (D) of all the coatings were calculated in Fig. 5. The lattice parameter (a) of CrN phase was about 0.1388 nm. The addition of V element decreased the lattice parameter of CrN. With the increase of V content, the lattice parameter of Cr-V-N coating with a high V content decreased and would be close to the lattice parameter of VN (a = 0.1376 nm). In addition, the EDS of S6 sample in Fig. 6 shows that it contained both Cr and V elements in a single grain. This further indicated that the Cr-V-N coatings were in the form of solid solution and the Cr lattice sites were substituted by V atoms. Similar results were reported in other Cr-V-N [13,16], Cr-Al-N [17], Cr-W-N [22] and Ti-Zr-N [23,24] coatings. The peak was broadened with a decrease of V content, which implied a

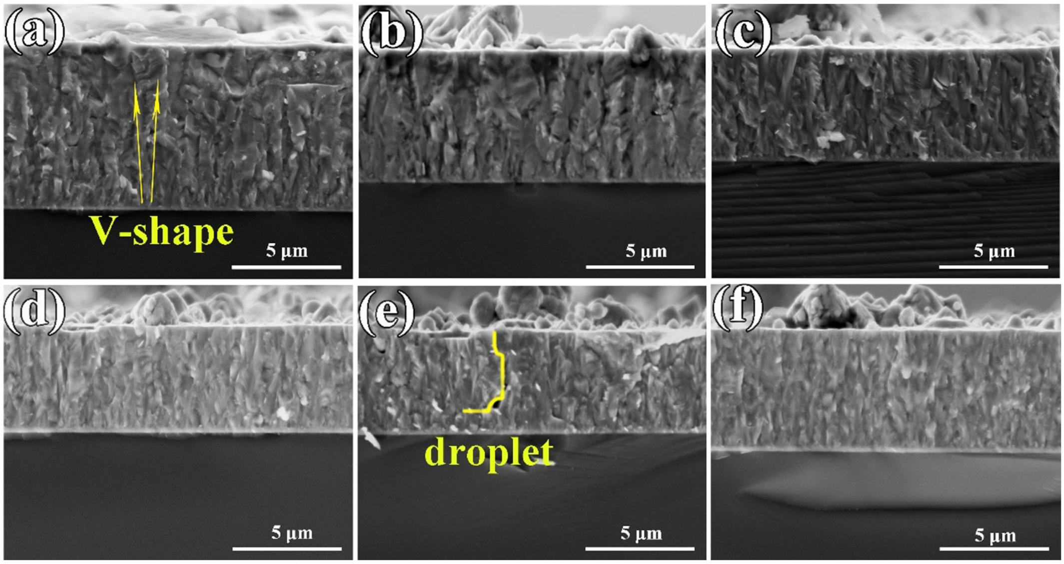

Fig. 3. Cross-sectional SEM micrographs of Cr-V-N coatings with different V contents: (a) S1 (0.32 at.%), (b) S2 (0.89 at.%), (c) S3 (4.46 at.%), (d) S4 (11.16 at.%), (e) S5 (16.55 at.%), (f) S6 (31.14 at.%).

lattice distortion or grain refining [25]. As shown in Fig. 5, the grain size of the S1–S5 enlarged with the increase of V content. Whereas, the S6 coating, with the broadest (111) peak, showed the minimum grain size. The full width at half maximum (FWHM) of (111) peak could be semi-qualitatively used to estimate the crystallinity. The smaller the FWHM was, the better the crystallinity could be. S6 coating with the highest V content presented weak crystallinity.

To further clarify the effect of V content on the microstructure of the coatings, detailed cross-sectional TEM micrographs of S3, S5 and S6 coatings were taken (Fig. 7). Both the S3 and S5 coatings had distinct columnar structure (Fig. 7a, Fig. 7d) with large grain size, whereas the S6 coating was featureless (Fig. 7g). The HRTEM image (Fig. 7b, Fig. 7e, Fig. 7h) of single grain showed the CrN phase only, neither V metal nor compound phase of V was found. The measured interplanar spacing of CrN (111) plane decreased with the increase of V content, which was in accord with the XRD observation. In addition, the HRTEM characterization revealed the weakest crystallinity of the S6 coating. The Cr (211) plane and CrN phase with several distinct orientations were observed in SAED patterns of S3 (Fig. 7c). This result demonstrated that the excess Cr existed in the form of Cr metal crystal in the coating. The

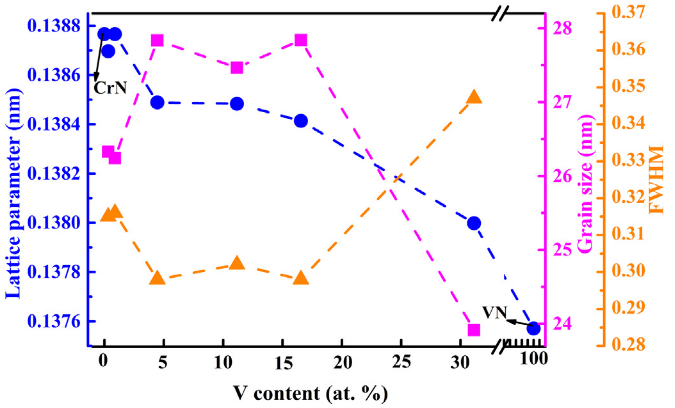

Fig. 5. Lattice parameters, grain size and FWHM of (111) peak for all the coatings S1–S6.

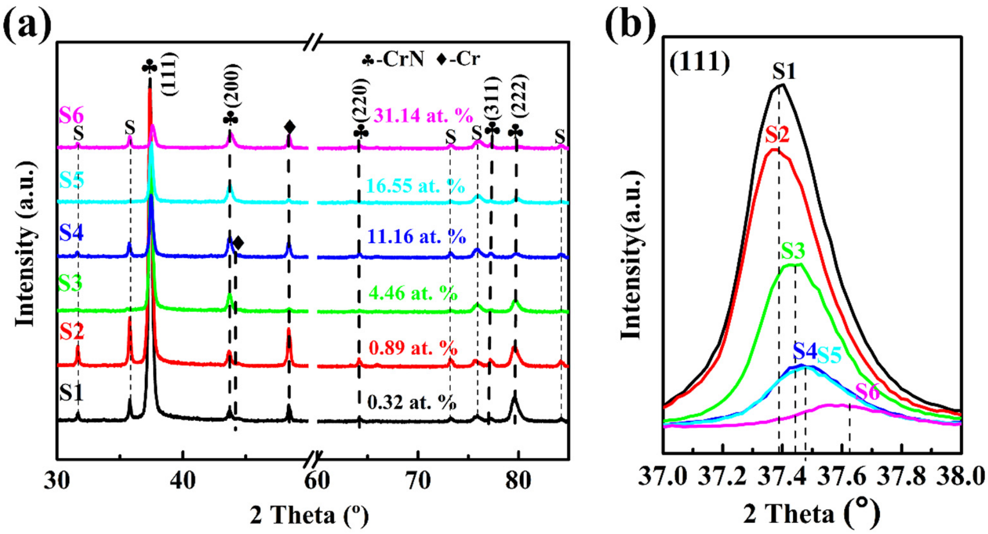

Fig. 4. X-ray diffraction pattern of Cr-V-N coatings with different V contents (a), and zoomed-in view of (111) peak (b).

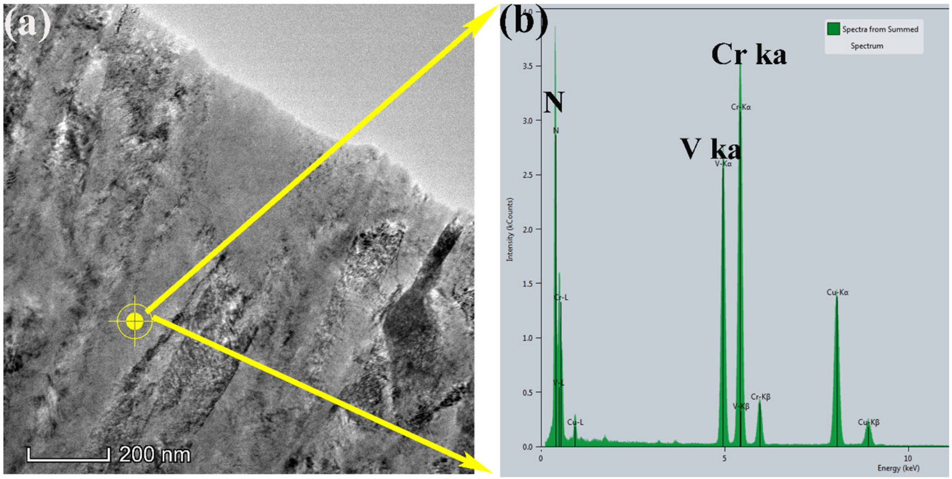

Fig. 6. (a)The TEM image of S6, and (b) the EDS of a single grain in S6.

CrN phase was also detected in the SAED patterns of S5 and S6 coatings, which indicated the CrN as the main phase component of the coatings. The continuous growth of the coarse grain in S5 coating was observed in the dark field TEM image in Fig. 8a. In contrast, the grain of S6 coating in Fig. 8b was manifested to be fine and discontinuous. Overall, an excess addition of V element into CrN weakened the crystallinity and made the coating grew in a way of discontinuous columnar structure.

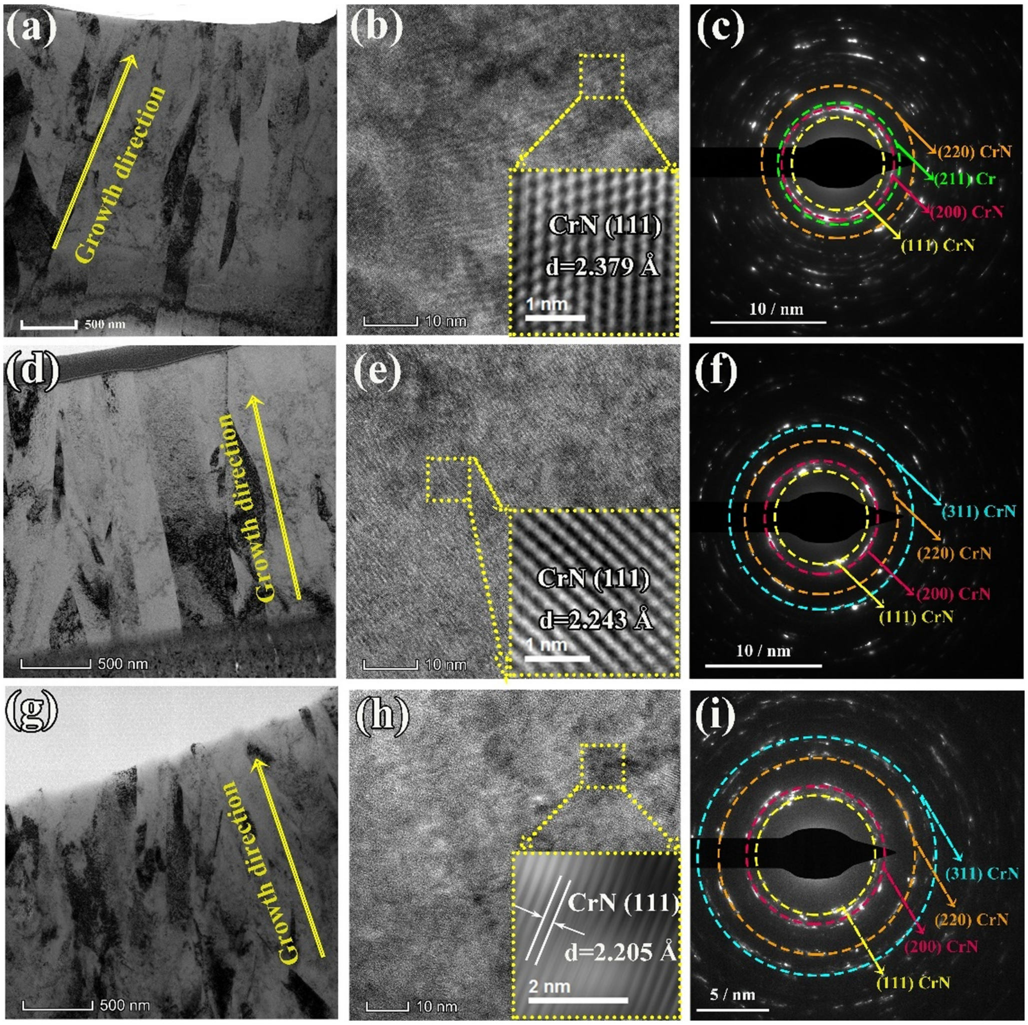

Fig. 7. Phase and microstructure of Cr-V-N coatings: (a), (d), (g) low-magnification overview image of S3 (4.46 at.%), S5(16.55 at.%), and S6 (31.14 at.%), respectively, and (b), (e), (h) corresponding HRTEM and inverse fast Fourier transform images, as well as (c), (f), (i) SAED patterns.

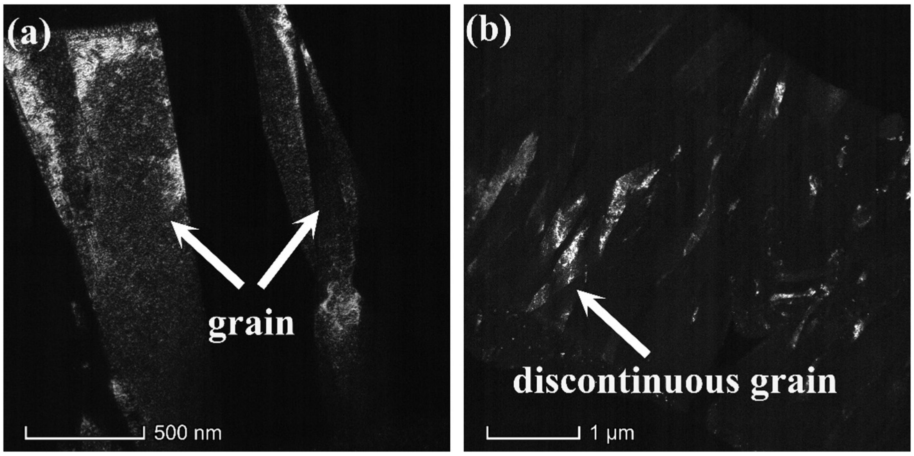

Fig. 8. The dark field TEM images of the cross-section of S5 (16.55 at.%) and S6 (31.14 at.%) coatings.

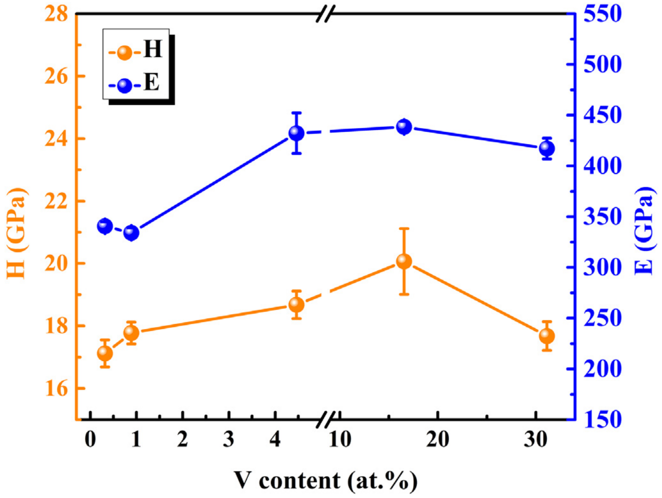

Fig. 9. H and E values of Cr-V-N coatings with different V contents.

3.2. Mechanical properties

The wear resistance of hard coatings can be indirectly evaluated from their hardness (H) and Young's modulus (E). In Fig. 9a, S5 showed the highest H and E of 20.1 ± 1.0 GPa and 438.5 ± 5.3 GPa, respectively. When V content increased from 0.32 at.% (S1) to 16.55 at.% (S5), a significant increase was observed in the H by ~17% and E by ~29%, respectively. However, as the V content continued to increase, the H and E declined. The solid solution with a certain amount of V content (< 16.55 at.%) into the CrN coating led to lattice distortion, which was beneficial to improve the hardness. But an excess of V content was detrimental to hardness due to the increased disorder caused by weak crystallinity.

Toughness means the strain-energy absorbing ability to create and propagate the crack [26–28]. Here, the toughness of S3 and S5 samples were assessed by the Vickers indentation test under a load of 5 N. From the SEM images of the indentations (Fig. 10), feeble edge cracks along the indentation circumference were visible for both coatings and radial cracks were almost inexistent, which implied their high damage resistance and good toughness.

The scratch test is commonly used to assess the adhesion between substrates and coatings. The cohesive strength failure that takes place inside the coating can also be evaluated. Fig. 11 shows the scratch track morphologies of Cr-V-N coatings on cemented-carbide substrates. The critical loads (Lc2) of S1, S3, S4, and S6 were determined to be about 105 N, 100 N, 98 N and 97 N, respectively. For S1 and S3 coating, the curved cracks inside the scratch were observed and the coating failure was caused by wedge spallation along the sides of the scratch (Fig. 11e-f). For S4 coating, circumferential cracks dominated the scratch and the fragment was depressed into the substrate surface (Fig. 11g). In these cases, the coatings all showed remarkable plastic deformation. Instead of conformal cracks, the failure mode of S6 coating was different from other coatings discussed above (Fig. 11h). Under the squeezing of moved diamond stylus, the coating showed good toughness with feeble spallation observed. The continuous ductile perforations generated inside the scratch track and the substrate material was exposed with depressed crushed coating fragments.

Above all, the coatings with different V contents showed excellent

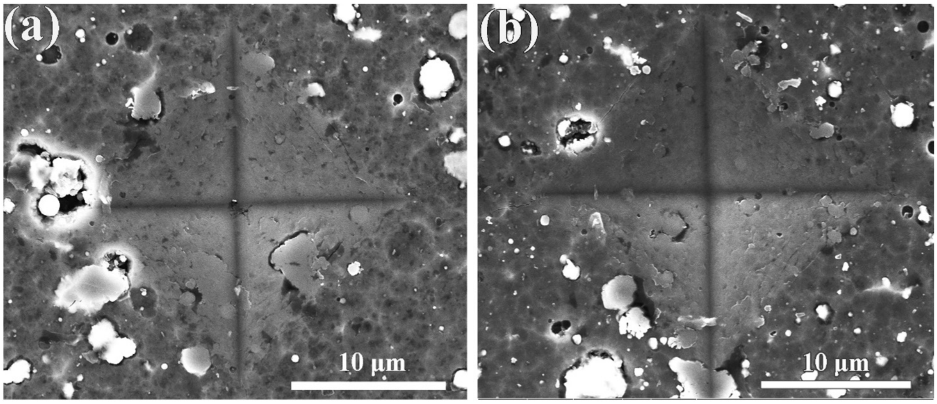

Fig. 10. SEM images of Vickers indentation for (a) S3 (4.46 at.%), and (b) S5 (16.55 at.%) coatings.

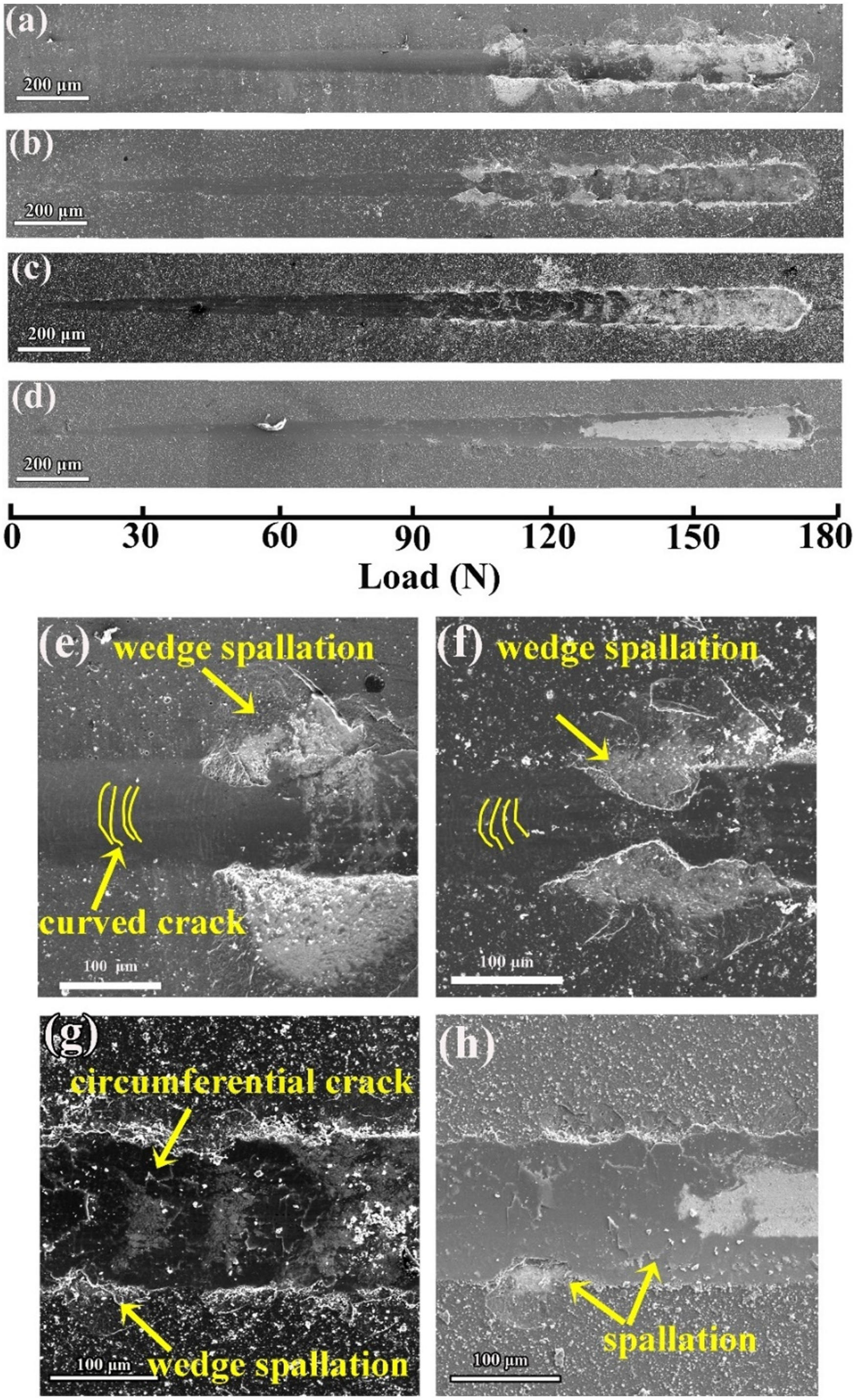

Fig. 11. Scratch tracks of Cr-V-N coatings with different V contents: (a) S1 (0.32 at.%), (b) S3 (4.46 at.%), (c) S4 (11.16 at.%), (d) S6 (31.14 at.%), and (e), (f), (g), (h) are enlarged images of crack propagation of S1, S3, S4, S6, respectively.

toughness and adhesion strength. When the V content was in the range of 0.32 at.% to 16.55 at.%, the solid solution strengthening effect was more prominent, the H and E were linearly elevated. When the V content was 31.14 at.%, the solid solution strengthening effect made no difference and the weak crystallinity caused by the increased disorder shed some light on the decreased H and E. It is predictable that the good mechanical properties will make a significant role to improve wear resistance of the coatings.

3.3. *Tribological behavior*

The friction curves of different V-containing coatings are shown in Fig. 12a. Firstly, the COF increased sharply and then decreased promptly within the running-in period for all curves. After the run-in period, the curves of S1, S2 and S3 showed great oscillation and there was a general increase with the extension of friction time, while S4–S6 showed comparatively stable trends. The average value of friction coefficients is shown in Fig. 12b. Overall, due to the solid solution strengthening effect, Cr-V-N coatings showed good tribological performance with the friction coefficient varying from 0.26 ± 0.01 to

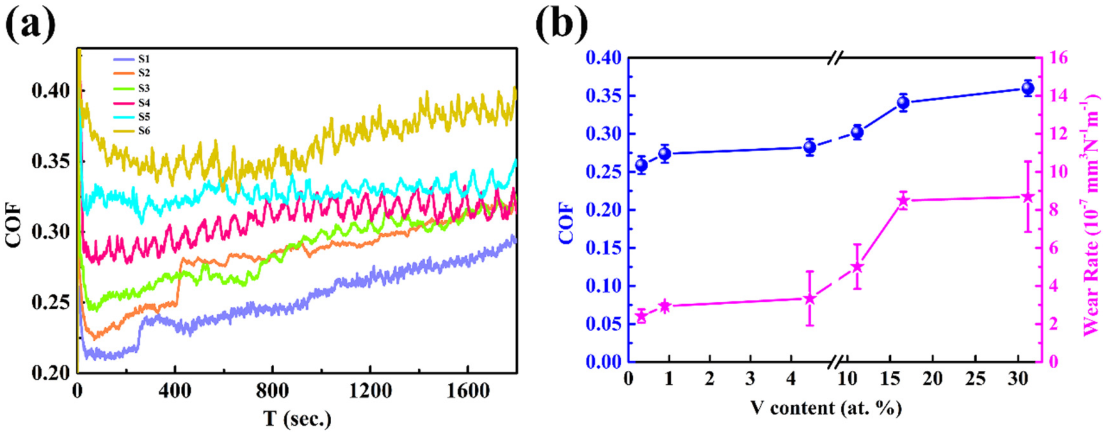

Fig. 12. (a) Sliding friction curves, (b) average friction coefficients and wear rates of Cr-V-N coatings sliding against Al_2O_3 balls in ambient air.

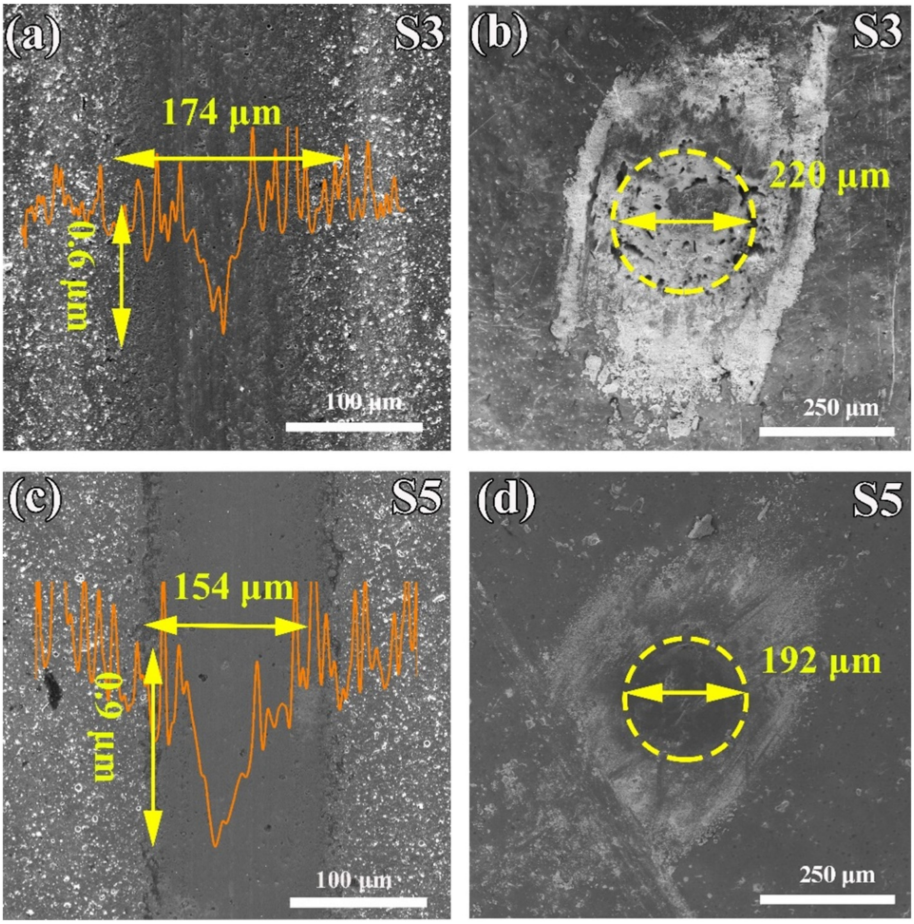

Fig. 13. SEM images of the wear tracks of Cr-V-N coatings (a) S3 (4.46 at.%), (c) S5 (16.55 at.%), and the corresponding wear scars of Al_2O_3 balls (b) S3, (d) S5.

0.36 ± 0.01, and wear rate in 10^{-7} mm^3N^{-1} m^{-1} order of magnitude. With the increase of the V content, both the average friction coefficient and the wear rate of the coatings increased progressively. The COF of S6 coating was 0.36 ± 0.01, 38% higher than that of S1. The hardness influenced by the solid solution was not the only factor determining the friction property, and the surface roughness (Ra) along with the crystallinity of the coating was also of great importance. Perfilyev et al. [14] reported that the roughness could influence the stick-slip event during friction. The rough surface led to high amplitude of friction force and prolonged the time of a single stick in the period of a single stick-slip event, thus contributed to the high friction. S1 coating, with relatively smooth surface, showed the lowest wear rate of 2.4 × 10^{-7} mm^3N^{-1} m^{-1}. With the increase of V content, the surface roughness Ra increased, thus leading to the increased wear rate. S6 coating, with high surface roughness and weak crystallinity, exhibited the highest wear rate of 8.7 × 10^{-7} mm^3N^{-1} m^{-1}, it was approximately four times higher than that of S1 coating.

The morphology of wear track and wear scars on Al_2O_3 balls were investigated to shed light on the friction mechanism, as shown in Fig. 13. In the wear track of S3 coating, shallow furrows parallel to the sliding direction and a great deal of white rod-like wear debris perpendicular to the sliding direction could be observed. The rod-like debris stemmed from the wear particles and was compressed by the sliding ball [3]. Compared with S3 coating, the wear track behaved

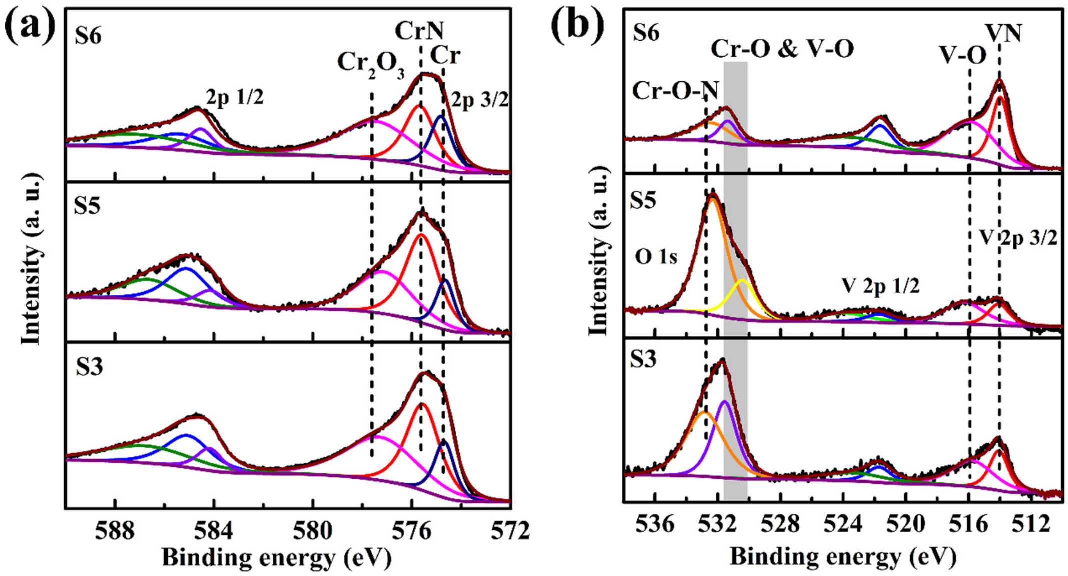

(c)

Sample ID.	Chemical composition (at. %)			
	Cr	V	N	O
S3	46	3	38	13
S6	25	19	38	17

Fig. 14. X-ray photoelectron spectroscopy spectra for the wear tracks of S3 (4.31 at.%), S5 (16.55 at.%) and S6 (31.14 at.%) sample: (a) Cr 2p, (b) V 2p & O 1 s, and (c) element contents of the wear track of S3 and S6.

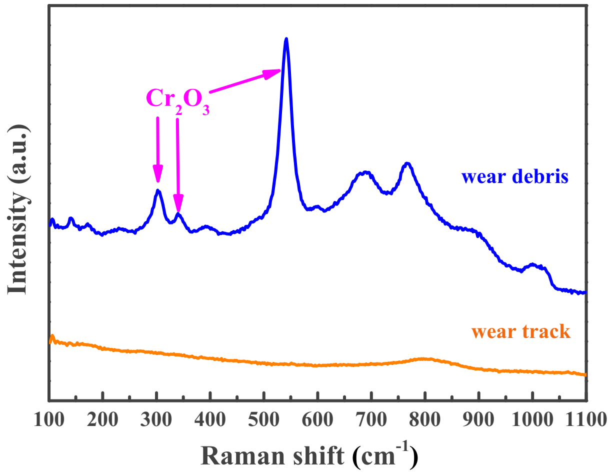

Fig. 15. Raman spectra of the wear debris (blue line) and wear track (yellow line) in S3 (4.31 at.%) coating. (For interpretation of the references to colour in this figure legend, the reader is referred to the web version of this article.)

narrower and deeper for S5 coating and the relatively little white rod-like wear debris with similar composition to those of S5 coating (49.79 at.% of Cr, 13.27 at.% of V, 33.09 at.% of N) were also detected by EDS spectrum analysis. The corresponding wear scars are also shown in Fig. 13. For S3, a large amount of wear debris accumulated and arranged along the sliding direction. The diameter of the wear scars on S3 and S5 coatings were measured to be 220 μm and 192 μm, respectively, However, the wear rate of S5 coating was 8.5 × 10^{-7} mm^3N^{-1} m^{-1}, 2.6 times higher than that of S3. The rough surface was detrimental to the friction that the effective contact area between rough peaks of the two relatively moving friction pairs got smaller, which in turn increased the pressure on the unit area. In addition, the exfoliated hard particles during friction played the role of abrasive wear. It ultimately increased the friction coefficient and aggravated the wear.

The XPS investigations in the wear track of S3, S5 and S6 samples were used to identify the chemical states. The use of C 1s level, associated with adventitious carbon as energy reference in XPS studies of nitride coatings, made an accurate identification of chemical state difficult [29]. The energy reference chosen in this paper was that of the Cr 2p level at 575.6 eV for CrN. As for the metallic constituents, the results of core level spectra Cr 2p and V 2p showed no significant differences. In case of Cr 2p (Fig. 14a) and V 2p (Fig. 14b), the 2p 1/2 and 2p 3/2 core level spectra were noticeable due to the spin-orbit coupling. For Cr $2p_{3/2}$, the peak centered at 574.3 eV and 576.2 eV were related to Cr metal and Cr_2O_3 [8], respectively. The peak at 514.2 eV and 515.8 eV of V $2p_{3/2}$ were referred to VN [17] and V-O [30], respectively. The O 1s spectrum (Fig. 14b) was fitted with two components at 532.1 eV and 530.6–532.4 eV, which were related to Cr-O-N [13], chromium and vanadium oxide bonds, respectively. The oxide phases detected in XPS resulted from the tribo-chemical reaction during the friction process and contaminations from the atmosphere [31]. In Fig. 14c, the O content in the wear track of S3 and S6 coating was 13 at.% and 17 at.%, respectively. In high V containing coatings, the content of oxide phases was low and the rate of tribo-chemical reaction was further limited.

The phase in the wear track and wear debris of S3 coating was tested using Raman spectroscopy method (Fig. 15). The Cr_2O_3 bands were not detected in the wear track of S3 coating, but clearly observed at 305 cm^{-1}, 343 cm^{-1}, 546 cm^{-1} [32] in the wear debris. The high temperature generated during the friction process induced the wear

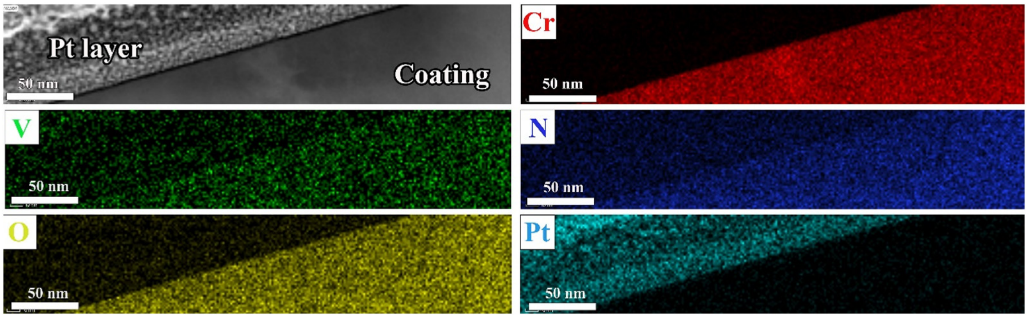

Fig. 16. Cross-sectional HRTEM image in the wear track center of S3 (4.31 at.%) coating with the corresponding EDS elemental mapping.

debris to oxidize rapidly, but it was less and played a minor role in lubrication. In order to further investigate the existence of oxide layer, the TEM sample was prepared by focused ion beam (FIB) in the wear track center of S3 coating. Fig. 16 shows the cross-sectional HRTEM image with corresponding EDS elemental mapping. The top layer of Pt was deposited to prevent the original information beneath the wear track being destroyed in the ion milling process. Thin oxide layers were not observed from TEM image. According to the results of XPS, Raman and TEM, it was confirmed that the tribo-chemical reaction during the friction process was sluggish. The detected oxide scales (such as V-O and Cr_2O_3) could partially influence the tribological behavior of Cr-V-N coating in this experiment, but the overall explanation of the friction mechanism needs to be combined with the microstructure and mechanical properties.

4. Conclusions

Anti-wear Cr-V-N solid solution coatings with different V contents were deposited by cathodic arc evaporation. The detailed microstructure, mechanical and tribological properties were evaluated. The incorporation of V increased the surface roughness of the coatings and weakened the crystallinity. Due to the solid solution strengthening effect, Cr-V-N coatings exhibited excellent adhesion strength as well as toughness, and also showed good wear resistance. As the V content increased, the COF and wear rate both showed a slight increase. The surface roughness and limited tribo-chemical reaction as well as crystallinity became the dominated reasons to affect the friction behaviors of different V contained coatings. In low V contained coatings, the surface was relatively smooth compared with other coatings. Cr_2O_3 and V-O oxides generated during friction process benefited the reduction of COF and wear rate. However, an excess addition of V element destroyed the original structure of CrN coating. The growth of the coating changed from continuous columnar to discontinuous columnar structure and the crystallinity was weakened. The weak crystallinity, rough surface and limited formation of oxide phases jointly led to the poor friction behavior of S6 coating. The lubricating oxide phase detected during the friction process were beneficial to reduce the friction coefficient. Whereas, the tribo-chemical reaction during the friction process at room temperature was sluggish and the oxidation of V was not obvious.

CRediT authorship contribution statement

Beibei Xu:Conceptualization, Methodology, Data curation, Software, Writing - original draft, Writing - review & editing.**Peng Guo**:Conceptualization, Writing - review & editing.**Zhenyu Wang**:Conceptualization, Writing - review & editing.**Rende Chen**:Data curation, Software.**Yumin Ye**:Data curation, Software.**Jintao Shuai**:Data curation, Software.**Aiying Wang**:Conceptualization, Methodology, Supervision.**Peiling Ke**:Conceptualization, Methodology, Writing - review & editing, Supervision, Funding acquisition.

Declaration of competing interest

We declare that we have no financial and personal relationships with other people or organizations that can inappropriately influence our work, there is no professional or other personal interest of any nature or kind in any product, service and/or company that could be construed as influencing the position presented in, or the review of, the manuscript entitled “Anti-wear Cr-V-N coating via V solid solution: microstructure, mechanical and tribological properties”.

Acknowledgments

This research was supported by the National Science and Technology Major Project (2017-VII-0013-0110), National Natural Science Foundation of China (51875555, 51901238).

References

[1] C. Meunier, S. Vives, G. Bertrand, X-ray diffractometry analysis of r.f.-magnetron-sputtered chromium/chromium nitride coatings, Surf. Coat. Technol. 107 (1998) 149–158.
[2] K. Ibrahim, M.M. Rahman, X.L. Zhao, J.P. Veder, Z.F. Zhou, E. Mohammadpour, R.H. Majeed, A.N. Nikoloski, Z.T. Jiang, Annealing effects on microstructural, optical, and mechanical properties of sputtered CrN thin film coatings: experimental studies and finite element modeling, J. Alloys Compd. 750 (2018) 451–464.
[3] Y.H. Cheng, T. Browne, B. Heckerman, Mechanical and tribological properties of CrN coatings deposited by large area filtered cathodic arc, Wear 271 (2011) 775–782.
[4] S.H. Wan, J.B. Pu, D.S. Li, G.A. Zhang, B. Zhang, A.K. Tieu, Tribological performance of CrN and CrN/GLC coated components for automotive engine applications, J. Alloys Compd. 695 (2017) 433–442.
[5] J. Xu, T. Oguchi, A.J. Freeman, Solid-solution strengthening: substitution of V in Ni_3Al and structural stability of Ni_3(Al,V), Phys. Rev. B Condens. Matter 36 (1987) 4186–4189.
[6] J.F. Smith, D.M. Bailey, O.N. Carlson, The Cr − V (chromium-vanadium) system, Journal of Phase Equilibria 2 (1982) 469–473.
[7] Z.Y. Wang, X.W. Li, X. Wang, S. Cai, P.L. Ke, A.Y. Wang, Hard yet tough V-Al-C-N nanocomposite coatings: microstructure, mechanical and tribological properties, Surf. Coat. Technol. 304 (2016) 553–559.
[8] W.B. Tian, Z.M. Sun, H.S. Hashimoto, Y.L. Du, Synthesis, microstructure and properties of $(Cr_{1-x}V_x)_2AlC$ solid solutions, J. Alloys Compd. 484 (2009) 130–133.
[9] F.L. Meng, Y.C. Zhou, J.Y. Wang, Strengthening of Ti_2AlC by substituting Ti with V, Scripta Mater 53 (2005) 1369–1372.
[10] M.W. Barsoum, I. Salama, T. El-Raghy, J. Golczewski, H.J. Seifert, F. Aldinger, W.D. Porter, H. Wang, Thermal and electrical properties of Nb_2AlC, (Ti, $Nb)_2AlC$ and Ti_2AlC, MMTA 33 (2002) 2775–2779.
[11] X.L. Ding, Y.Z. Zhan, H.Q. Tang, Development of $CoCrFeNiVAl_x$ high-entropy alloys based on solid solution strengthening, JOM 71 (2019) 3473–3480.
[12] S.S. Wo, Z.Y. Huang, L.P. Cai, W.Q. Hu, Y.B. Wang, Y. Zhou, H.X. Zhai, High strengthening effects and excellent wear resistance of $Ti_3Al(Si)C_2$ solid solutions, Int. J. Appl. Ceram. Tec. 16 (2019) 2398–2408.
[13] L. Aissani, C. Nouveau, M.J. Walock, H. Djebaili, A. Djelloul, Influence of vanadium on structure, mechanical and tribological properties of CrN coatings, Surf. Eng. 31 (2015) 779–788.
[14] V. Perfilyev, A. Moshkovich, I. Lapsker, A. Laikhtman, L. Rapoport, The effect of vanadium content and temperature on stick–slip phenomena under friction of CrV(x)N coatings, Wear 307 (2013) 44–51.
[15] L. Rapoport, A. Moshkovich, V. Perfilyev, I. Lapsker, M. Kugler, A. Kailer, A. Renz, T. Hollstein, High temperature friction behavior of CrVxN coatings, Surf. Coat.

Technol. 238 (2014) 207–215.

[16] M. Uchida, N. Nihira, A. Mitsuo, K. Toyoda, K. Kubota, T. Aizawa, Friction and wear properties of CrAlN and CrVN films deposited by cathodic arc ion plating method, Surf. Coat. Technol. 177-178 (2004) 627–630.

[17] Y.X. Qiu, S. Zhang, J.W. Lee, B. Li, Y.X. Wang, D.L. Zhao, Self-lubricating CrAlN/VN multilayer coatings at room temperature, Appl. Surf. Sci. 279 (2013) 189–196.

[18] L.V. Azaroff, Elements of X-Ray Crystallography, McGraw-Hill, New York, 1968.

[19] W.C. Oliver, G.M. Pharr, An improved technique for determining hardness and elastic modulus using load and displacement sensing indentation experiments, J. Mater. Res. 7 (2011) 1564–1583.

[20] D.J. Branes, J.E. Wilson, F.H. Stott, G.C. Wood, The influence of oxide films on the friction and wear of Fe-5% Cr alloy in controlled environments, Wear 45 (1977) 161–176.

[21] I. Petrov, P.B. Barna, L. Hultman, J.E. Greene, Microstructural evolution during film growth, J. Vac. Sci. Technol. A 21 (2003) S117–S128.

[22] F.B. Wu, S.K. Tien, J.G. Duh, Manufacture, microstructure and mechanical properties of CrWN and CrN/WN nanolayered coatings, Surf. Coat. Technol. 200 (2005) 1514–1518.

[23] G. Abadias, V.I. Ivashchenko, L. Belliard, et al., Structure, phase stability and elastic properties in the $Ti_{1-x}Zr_xN$ thin-film system: experimental and computational studies, Acta Mater. 60 (2012) 5601–5614.

[24] E.J. Herrera-Jimenez, A. Raveh, T. Schmitta, et al., Solid solution hardening in nanolaminate ZrN-TiN coatings with enhanced wear resistance, Thin Solid Films 688 (2019) 137431.

[25] H.J. Mei, Q.S. Luo, X.L. Huang, J.C. Ding, T.F. Zhang, Q.M. Wang, Influence of lubricious oxides formation on the tribological behavior of Mo-V-Cu-N coatings deposited by HIPIMS, Surf. Coat. Technol. 358 (2019) 947–957.

[26] J. Musil, Hard nanocomposite coatings: thermal stability, oxidation resistance and toughness, Surf. Coat. Technol. 207 (2012) 50–65.

[27] M.A. Meyers, L.E. Marr, Shock waves and high-strain-rate phenomena in metals, J. Appl. Mech. 49 (1982) 398–399.

[28] C.Q. Dang, J.L. Li, Y. Wang, J.M. Chen, Structure, mechanical and tribological properties of self-toughening TiSiN/Ag multilayer coatings on Ti6Al4V prepared by arc ion plating, Appl. Surf. Sci. 386 (2016) 224–233.

[29] G. Greczynski, L. Hultman, Reliable determination of chemical state in x-ray photoelectron spectroscopy based on sample-work-function referencing to adventitious carbon: resolving the myth of apparent constant binding energy of the C 1s peak, Appl. Surf. Sci. 451 (2018) 99–103.

[30] J. Mendialdua, R. Casanova, Y. Barbaux, XPS studies of V_2O_5, V_6O_{13}, VO_2 and V_2O_3, J. Electron. Spectrosc. 71 (1995) 249–261.

[31] R. Franz, J. Neidhardt, B. Sartory, R. Tessadri, C. Mitterer, Micro- and bonding structure of arc-evaporated AlCrVN hard coatings, Thin Solid Films 516 (2008) 6151–6157.

[32] C.P. Constable, J. Yarwood, P. Hovsepian, L.A. Donohue, D.B. Lewis, W.D. Münz, Structural determination of wear debris generated from sliding wear tests on ceramic coatings using Raman microscopy, J. Vac. Sci. Technol. A 18 (2000) 1681–1689.